© 2022. Published by The Company of Biologists Ltd | Journal of Cell Science (2022) 135, jcs259471. doi:10.1242/jcs.259471

SHORT REPORT

Angiomotin isoform 2 promotes binding of PALS1 to KIF13B at primary cilia and regulates ciliary length and signaling

Stine Kjær Morthorst[1,‡], Camilla Nielsen[1,‡], Pietro Farinelli[1,‡], Zeinab Anvarian[1], Christina Birgitte R. Rasmussen[1], Andrea Serra-Marques[2,*], Ilya Grigoriev[2], Maarten Altelaar[3], Nicoline Fürstenberg[1], Alexander Ludwig[4], Anna Akhmanova[2], Søren Tvorup Christensen[1,§] and Lotte Bang Pedersen[1,§]

ABSTRACT

The kinesin-3 motor KIF13B functions in endocytosis, vesicle transport and regulation of ciliary length and signaling. Direct binding of the membrane-associated guanylate kinase (MAGUK) DLG1 to the MAGUK-binding stalk domain of KIF13B relieves motor autoinhibition and promotes microtubule plus-end-directed cargo transport. Here, we characterize angiomotin (AMOT) isoform 2 (p80, referred to as Ap80) as a novel KIF13B interactor that promotes binding of another MAGUK, the polarity protein and Crumbs complex component PALS1, to KIF13B. Live-cell imaging analysis indicated that Ap80 is concentrated at and recruits PALS1 to the base of the primary cilium, but is not a cargo of KIF13B itself. Consistent with a ciliary function for Ap80, its depletion led to elongated primary cilia and reduced agonist-induced ciliary accumulation of SMO, a key component of the Hedgehog signaling pathway, whereas Ap80 overexpression caused ciliary shortening. Our results suggest that Ap80 activates KIF13B cargo binding at the base of the primary cilium to regulate ciliary length, composition and signaling.

KEY WORDS: Angiomotin p80, KIF13B, PALS1, Primary cilia

INTRODUCTION

Kinesin-3 family members are processive microtubule plus-end-directed motors involved in vesicle transport and endocytosis (Siddiqui and Straube, 2017). The kinesin-3 member KIF13B (or guanylate kinase-associated kinesin; GAKIN) was initially identified as an interactor of DLG1, a Scribble polarity complex component of the membrane-associated guanylate kinase (MAGUK) homologue family in lymphocytes (Hanada et al., 2000). Subsequent studies implicated KIF13B in the regulation of neuronal polarity, axon formation and myelination (Horiguchi et al., 2006; Yoshimura et al., 2010; Bolis et al., 2009; Noseda et al., 2016); CAV1-dependent endocytosis of LRP1 and cholesterol in hepatocytes (Kanai et al., 2014; Mills et al., 2019); Golgi to plasma membrane trafficking of VEGFR2 in endothelial cells (Yamada et al., 2014) and trafficking of RAB6A exocytotic vesicles in HeLa cells (Serra-Marques et al., 2020); germ cell migration and planar cell polarity signaling in *Xenopus laevis* (Tarbashevich et al., 2011; Ossipova et al., 2015); and regulation of ciliary CAV1 distribution and Sonic hedgehog (SHH) signaling in hTERT-immortalized retinal pigment epithelial (RPE1) cells (Schou et al., 2017).

KIF13B activation and function are regulated by binding partners that control its conformation and dimerization (Soppina et al., 2014; Siddiqui and Straube, 2017; Morthorst et al., 2018; Ren et al., 2018). The best-characterized KIF13B regulator and cargo is DLG1, which binds directly to the MAGUK-binding stalk (MBS) domain of KIF13B to relieve motor autoinhibition and promote KIF13B-mediated transport of DLG1 along microtubules (Hanada et al., 2000; Asaba et al., 2003; Yamada et al., 2007; Zhu et al., 2016). Similarly, other MAGUKs including DLG4 and PALS1, a Crumbs polarity complex component, bind directly to the MBS domain of KIF13B (Zhu et al., 2016). Furthermore, we previously identified an interaction between KIF13B and the ciliary transition zone (TZ) protein NPHP4 (Schou et al., 2017), which also associates with PALS1 and PATJ (Sang et al., 2011; Delous et al., 2009). Whether the interaction between KIF13B and PALS1 is relevant in a ciliary context is unknown.

Primary cilia are microtubule-based sensory organelles on the cell surface (Anvarian et al., 2019) that coordinate signaling pathways, for example, Shh signaling (Bangs and Anderson, 2017). The ciliary axoneme extends from the basal body and is surrounded by a membrane that is compositionally distinct from the plasma membrane. Ciliary compartmentalization and function are regulated by the TZ at the ciliary base (Garcia-Gonzalo and Reiter, 2017), and by intraflagellar transport (IFT), which moves trains of IFT particles containing ciliary cargoes in and out of the cilium via the kinesin-2 and dynein-2 motors, respectively (Taschner and Lorentzen, 2016). Additionally, the nematode kinesin-3 motor KLP-6 regulates neuronal ciliary composition and function by promoting the release of extracellular vesicles from cilia (Akella and Barr, 2021). Recently, we demonstrated that KIF13B moves bidirectionally within the primary cilia of RPE1 cells (Juhl et al., 2023), but how KIF13B intraciliary movement is regulated and the identity of the ciliary cargoes of KIF13B are unknown.

Here, we characterize angiomotin (AMOT) isoform 2 (p80, hereafter referred to as Ap80) as a KIF13B interactor and show that Ap80 promotes binding of KIF13B to PALS1. Ap80 is concentrated at and recruits PALS1 to the ciliary base of RPE1 cells. Depletion of Ap80 caused ciliary elongation and reduced agonist-induced ciliary

[1]Department of Biology, University of Copenhagen, Universitetsparken 13, DK-2100 Copenhagen Ø, Denmark. [2]Cell Biology, Neurobiology and Biophysics, Department of Biology, Faculty of Science, Utrecht University, 3584 CH Utrecht, The Netherlands. [3]Biomolecular Mass Spectrometry and Proteomics, Bijvoet Center for Biomolecular Research and Utrecht Institute for Pharmaceutical Sciences, Utrecht University, Padualaan 8, 3584 CH Utrecht, The Netherlands. [4]School of Biological Sciences and NTU Institute of Structural Biology, Nanyang Technological University, Singapore City 637551, Singapore.
*Present address: Immunology Discovery, Genentech, Inc., South San Francisco, CA 94080-4990, USA.
‡These authors contributed equally to this work

§Authors for correspondence (stchristensen@bio.ku.dk; lbpedersen@bio.ku.dk)

A.S.-M., 0000-0003-4215-3024; M.A., 0000-0001-5093-5945; A.L., 0000-0002-0696-5298; A.A., 0000-0002-9048-8614; S.T.C., 0000-0002-7067-5586; L.B.P., 0000-0002-9749-3758

Handling Editor: David Stephens
Received 26 October 2021; Accepted 16 May 2022

Journal of Cell Science (2022) 135, jcs259471. doi:10.1242/jcs.259471

accumulation of SMO, a key SHH pathway component, whereas Ap80 overexpression caused ciliary shortening. We propose that Ap80 activates KIF13B cargo binding at the base of the primary cilium to regulate ciliary length, composition and signaling.

RESULTS AND DISCUSSION

KIF13B interacts with the N-terminus of Ap80

To identify KIF13B interactors, we performed streptavidin pull-down assays with BirA- and GFP-tagged (BirAGFP) KIF13B constructs combined with mass spectrometry (MS) (Table 1). We used the deletion mutants BirAGFP–KIF13B Tail 2 (residues 607–1826) and BirAGFP–KIF13B Tail 3 (residues 752–1826), which contain and lack the MBS domain, respectively (Serra-Marques et al., 2020), reasoning that these might reveal MBS-specific interactors. We identified several proteins that had significant hits with more peptides in the Tail 2 pull-down sample compared to the Tail 3 pull-down sample (Table 1). These included DLG1 and its known interactors MPP7, LIN7C and CASK (Bohl et al., 2007; Lee et al., 2002), and utrophin (UTRN), a large cytoskeletal adaptor that binds to KIF13B in a complex that mediates the endocytosis of LRP1 (Kanai et al., 2014). Known interactors of UTRN, SNTB2 (Kramarcy et al., 1994) and dystrobrevins (Peters et al., 1997), were also present in the pull down. The most prominent, potential, novel interactors of KIF13B, showing significantly stronger association with Tail 2 compared to Tail 3, were the kinase D-interacting substrate of 220 kDa (KIDINS220), a conserved transmembrane molecule implicated in signaling (Neubrand et al., 2012), and an adaptor protein belonging to the motin family, angiomotin (AMOT) (Moleirinho et al., 2014) (Table 1).

Table 1. Binding partners of the indicated BirAGFP–KIF13B constructs in HEK293T cells identified by mass spectrometry analysis

		KIF13B Tail 2		KIF13B Tail 3	
Gene name*	Protein ID*	Unique peptides	PSM	Unique peptides	PSM
KIF13B	Q9NQT8	147	294	102	177
MOV10	Q9HCE1	27	27	24	24
MARK2	Q7KZI7	26	31	17	19
HSPA5	P11021	22	24	16	18
KIDINS220	**Q9ULH0**	**22**	**22**	**8**	**8**
HADHA	P40939	20	21	11	11
UTRN	**P46939**	**19**	**19**	**2**	**2**
LRPPRC	P42704	17	17	10	10
MARK3	P27448	16	18	17	18
CUL3	Q13618	16	17	12	13
DLG1	**Q12959**	**15**	**16**	**0**	**0**
AMOT	**Q4VCS5**	**14**	**15**	**0**	**0**
MARK1	Q9P0L2	12	12	6	6
HADHB	P55084	11	12	10	10
ATAD3C	Q5T2N8	11	11	10	11
SNTB2	**Q13425**	**11**	**11**	**4**	**4**
NCL	P19338	9	9	9	9
MPP7	**Q5T2T1**	**9**	**9**	**0**	**0**
KLHL12	Q53G59	8	9	7	7
OSBPL8	Q9BZF1	8	9	5	5
PPP2R1A	P30153	5	5	4	4
ILF2	Q12905	5	7	3	3
CCT6A	P40227	5	5	3	3
TCP1	P17987	5	5	3	3
HNRNPH1	**P31943**	**5**	**5**	**2**	**2**
RPS11	**P62280**	**5**	**5**	**1**	**1**
PPP2R2A	**P63151**	**5**	**6**	**1**	**1**
CCT4	P50991	4	4	4	4
HNRNPA1	P09651	4	4	4	4
PKN3	Q6P5Z2	4	4	4	4
CSNK2A1	P68400	4	4	3	3
DDX6	P26196	4	4	3	3
LRRC59	Q96AG4	4	4	2	2
LIN7C	**Q9NUP9**	**4**	**4**	**0**	**0**
PDP1	**Q9P0J1**	**4**	**4**	**0**	**0**
CASK	**O14936**	**4**	**4**	**0**	**0**
KLHL7	Q8IXQ5	3	3	2	2
FAM98A	Q8NCA5	3	3	2	2
CCT7	Q99832	3	4	1	1
AIFM1	O95831	3	3	1	1
IRS4	O14654	3	3	1	1
DDX3X	O00571	3	3	1	1
DTNB	**O60941**	**3**	**4**	**0**	**0**
FBXW11	Q9UKB1	3	3	0	0
XPR1	Q9UBH6	3	3	0	0
DTNA	**Q9Y4J8**	**3**	**3**	**0**	**0**
CEP104	O60308	3	3	0	0
GLG1	Q92896	3	3	0	0

*The genes/proteins indicated in bold preferentially bind KIF13B Tail 2 over Tail 3 and are discussed in the text. Only proteins identified by at least three unique peptides in the BirAGFP–KIF13B Tail 2 sample are included. PSM, peptide spectrum matches.

We focused on AMOT due to its reported interaction with PALS1 (Wells et al., 2006; Tan et al., 2020), which associates with KIF13B (Zhu et al., 2016) and the KIF13B interactor NPHP4 (Delous et al., 2009; Schou et al., 2017). AMOT is found in two splice variants; angiomotin isoform 1 (p130 or Ap130) contains a 409-amino-acid N-terminal extension that is absent in isoform 2, p80 or Ap80 (Ernkvist et al., 2006). We previously reported that KIF13B binds Ap80 (Schou et al., 2017), but the interaction had not been characterized in detail. We confirmed by using immunoprecipitation (IP) of FLAG-tagged proteins (i.e. FLAG IP) in human embryonic kidney cells expressing SV40 large T antigen (HEK293T) that FLAG–Ap80 interacts with HA-tagged full-length or motorless KIF13B (KIF13B-Δmotor–HA; residues 393–1826), but FLAG–Ap130 does not (Fig. 1A). Supporting this finding, FLAG–Ap80 co-immunoprecipitated with GFP–KIF13B (Fig. 1B). IP experiments using different FLAG–Ap80 truncations identified the first 34 residues in Ap80 to be essential for KIF13B binding, as Ap80-NB (residues 1–245), comprising the N-terminus and BAR domain, bound to KIF13B-Δmotor–HA, whereas Ap80-B (residues 35–245) did not (Fig. 1C,D). Ap80 residues 1–245 are also present in Ap130, which failed to bind KIF13B (Fig. 1A,C), suggesting that the KIF13B binding site in AMOT is blocked by the Ap130 N-terminal domain.

Ap80 interacts with the stalk and tail region of KIF13B and promotes KIF13B–PALS1 association

To map the Ap80-NB-binding region of KIF13B, we generated plasmids encoding GFP–KIF13B truncations that deleted most of the C-terminal stalk and tail region (Fig. 2A; Schou et al., 2017). Co-expression with FLAG–Ap80-NB followed by FLAG IP identified KIF13B residues 561–1500 (GFP–Tail 11) as the minimal Ap80-NB binding site in KIF13B (Fig. 2B; Fig. S1A,B), and a reciprocal GFP IP confirmed this result (Fig. S1C). Full-length FLAG–Ap80 interacted with an even shorter KIF13B fusion, GFP–Tail 8, which contains the MBS domain but lacks residues 1327–1500 that are present in GFP–Tail 11 (Fig. 2A,C; Fig. S1D), suggesting that the MBS domain is necessary for interaction with Ap80-NB and that residues 1327–1500 are also important for binding. However, the latter region is dispensable for interaction with full-length Ap80. These results are consistent with our MS data as the sequences of Tail 8 and Tail 11 are found within the BirAGFP–KIF13B Tail 2 fusion protein that interacts

Journal of Cell Science (2022) 135, jcs259471. doi:10.1242/jcs.259471

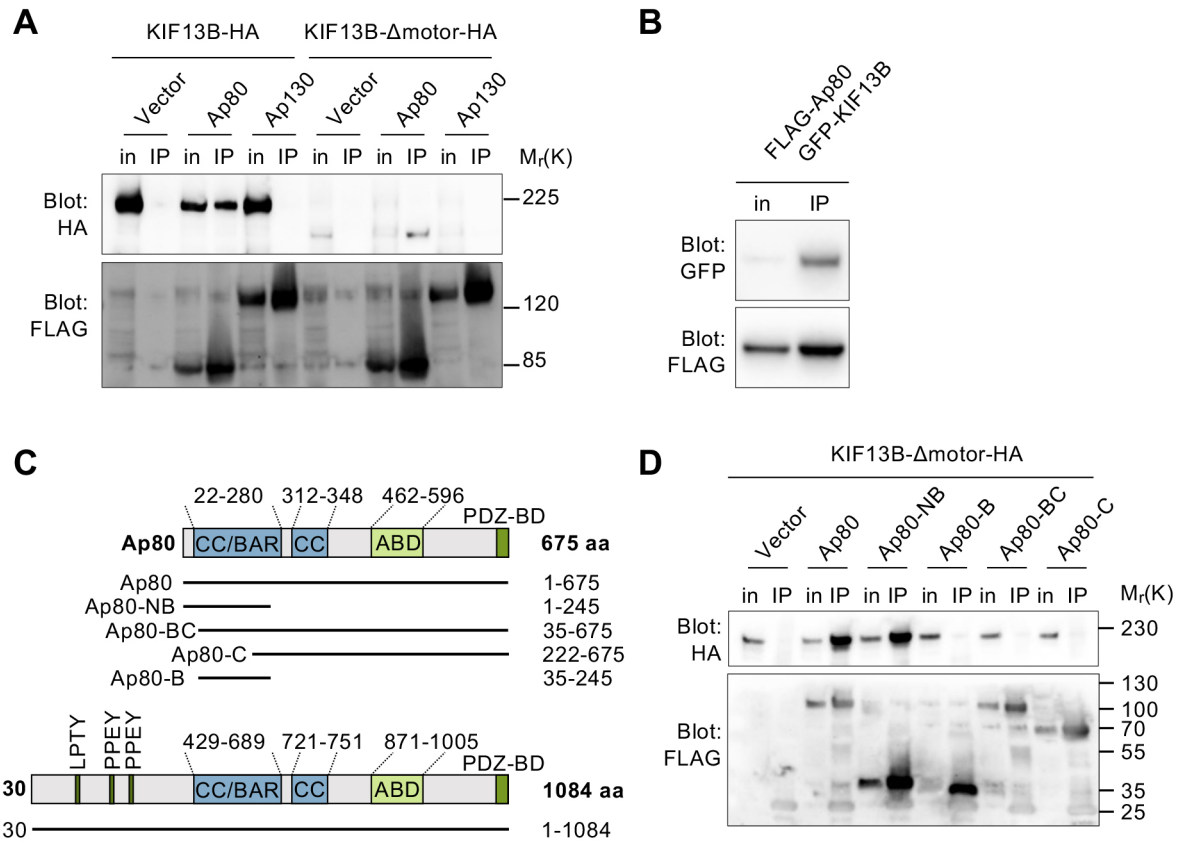

Fig. 1. Ap80 interacts with KIF13B via its N-terminus. (A) Representative images of immunoblotting following FLAG IP of cells co-expressing FLAG-tagged Ap80 or Ap130 fusion proteins and KIF13B–HA or KIF13B-Δmotor–HA. (B) Representative images of immunoblotting following GFP IP of cells co-expressing FLAG–Ap80 and GFP–KIF13B. The input (in) and IP pellet (IP) fractions were subjected to immunoblotting using the indicated antibodies. (C) Diagram of full-length Ap80 and Ap130 and the FLAG–Ap80 truncations used. ABD, angiostatin binding domain; CC, coiled coil; CC/BAR, coiled-coil/BAR domain; PDZ-BD, PDZ-binding domain. (D) Representative images of immunoblotting following FLAG IP of cells co-expressing FLAG-tagged Ap80 or Ap80 truncations and KIF13B-Δmotor–HA. Images are representative of at least three independent IP experiments.

with AMOT (Table 1; Serra-Marques et al., 2020). Additionally, immunofluorescence microscopy (IFM) of RPE1 cells co-expressing FLAG–Ap80-NB or FLAG–Ap80 with different GFP–KIF13B truncations showed that those binding to FLAG–Ap80-NB (e.g. Tails 7 and 11) or FLAG–Ap80 (Tail 8) in the IP experiments (Fig. 2B,C) also colocalize with these fusion proteins, whereas non-binding truncations (e.g. Tails 9 and 12) do not (Fig. S1E,F). Co-expression of FLAG–Ap80 with Ap80-binding GFP–KIF13B truncations increased the total cellular number of FLAG–Ap80-positive vesicles (Fig. S1G), possibly due to their fission.

The MBS domain of KIF13B binds directly to the guanylate kinase domains of DLG1, DLG4 and PALS1 (Yamada et al., 2007; Zhu et al., 2016), whereas residues 1327–1500 bind MARK2 (Yoshimura et al., 2010). We therefore asked whether Ap80 binds KIF13B indirectly via these proteins. However, GFP–DLG1 and GFP–MARK2 did not co-immunoprecipitate with FLAG–Ap80, whereas HA–PALS1 did (Fig. 2D; Fig. S2A). PALS1 binds to the C-terminus of Ap80 (Fig. 2E; Fig. S2A), whereas KIF13B binds to its N-terminus (Ap80-NB; Fig. 1C,D). Thus, Ap80 interacts independently with both KIF13B and PALS1. HA–PALS1 did not co-immunoprecipitate with motorless KIF13B (GFP–KIF13B-Δmotor) alone, but did upon simultaneous co-expression with FLAG–Ap80 (Fig. 2F). Similar results were obtained with full-length GFP–KIF13B (Fig. S2B). The inability of PALS1 to bind full-length or motorless KIF13B could be due to an intramolecular interaction in KIF13B blocking access to the MBS domain. Supporting this hypothesis, IP using GFP–KIF13B or HA–KIF13B truncations revealed that KIF13B residues 1289–1499 interact with the MBS domain (Fig. S2C,D), consistent with previous work (Yamada et al., 2007). This suggests that Ap80 promotes association of PALS1 with KIF13B by inducing a conformational change in KIF13B that allows PALS1 to access the MBS region.

Our protein interaction data are summarized in Fig. 2G. First, we suggest that the interaction between the NB region of Ap80 and the MBS domain in KIF13B (indicated by ‘a’ in Fig. 2G) is necessary, but not sufficient for these proteins to interact. Two additional supporting interactions can occur: one between the Ap80 NB region and KIF13B residues 1327–1500 (indicated by ‘b’), which seem important for strong binding, and another between the MBS domain and the C-terminus of Ap80 (indicated by ‘c’), likely mediated by PALS1. Binding of Ap80 to KIF13B presumably induces a conformational change in KIF13B that permits binding of the MBS domain to PALS1.

Colocalization of Ap80, PALS1 and KIF13B at the primary cilia base

Next, we asked whether Ap80, KIF13B and PALS1 colocalize in cells. First, we examined endogenous levels of Ap80 and Ap130 in mouse fibroblasts (NIH3T3 cells) and different mouse or human epithelial cell lines (IMCD3, HEK293T and RPE1) by immunoblotting using the antibody against AMOT (Fig. S3A). We chose RPE1 cells for further analysis as they specifically expressed

Journal of Cell Science (2022) 135, jcs259471. doi:10.1242/jcs.259471

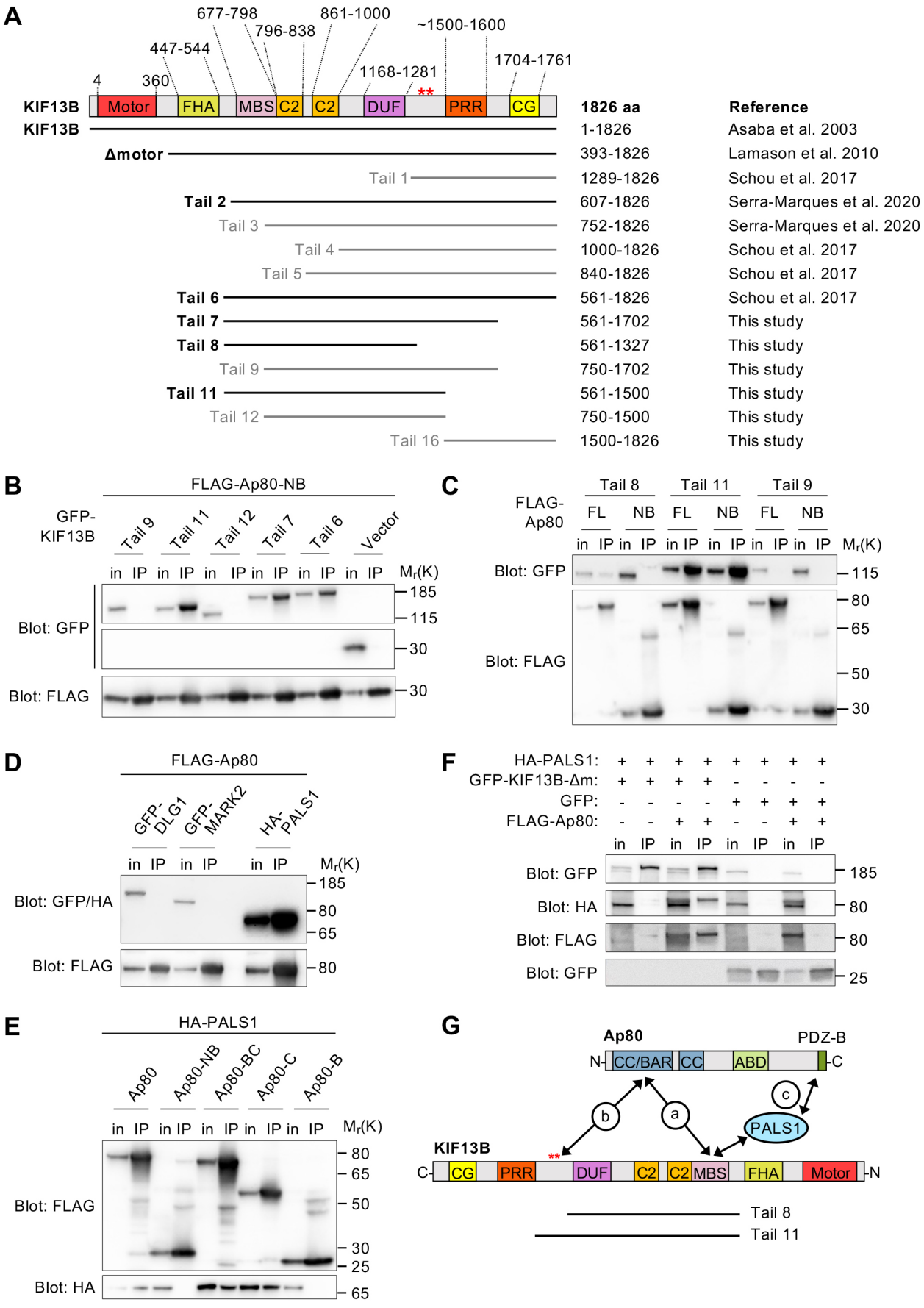

Fig. 2. See next page for legend.

Journal of Cell Science

Fig. 2. Ap80 binds the KIF13B tail region and promotes KIF13B–PALS1 association. (A) Diagram of full-length and truncated KIF13B fusion proteins; those binding to Ap80 are indicated in bold. CG, CAP-Gly domain; DUF, domain of unknown function; FHA, Forkhead-associated domain; PRR, proline-rich region; red asterisks indicate MARK2 phosphorylation sites (Yoshimura et al., 2010; Soppina et al., 2014; Yamada et al., 2014; Zhu et al., 2016; Schou et al., 2017). (B) Representative images of immunoblotting following FLAG IP of cells co-expressing FLAG–Ap80-NB and GFP (empty vector) or different GFP–KIF13B truncations. The input (in) and IP pellet (IP) fractions were analyzed by immunoblotting using the indicated antibodies. (C–F) Representative images of immunoblotting following FLAG (C–E) or GFP (F) IP of cells expressing the indicated fusion proteins, analyzed with the indicated antibodies. GFP–KIF13BΔm indicates GFP–KIF13B-Δmotor. Images are representative of at least three independent IP experiments. (G) Model for Ap80–KIF13B interaction.

Ap80 but not Ap130. In RPE1 cells, Ap80 and KIF13B were upregulated by high cell confluency and serum deprivation (Fig. S3A), conditions that promote ciliogenesis (Pugacheva et al., 2007) and in which GFP–KIF13B localizes to and moves within cilia (Schou et al., 2017; Juhl et al., 2023). In live ciliated RPE1 cells stably expressing the ciliary membrane marker SMO–tRFP (Lu et al., 2015), GFP-tagged Ap80 was concentrated at the base of the cilium in most cells (89±8%, indicated as mean±s.d.; n=67 cells) and exhibited little, if any, movement (Fig. 3A; Fig. S3G; Movie 1), even when co-expressed with mCherry–KIF13B, which colocalized with Ap80–GFP at the centrosomes (Movies 2 and 3). However, we cannot rule out the possibility that the GFP tag affects Ap80 mobility. In fixed cells, FLAG–Ap80 and FLAG–Ap80-NB were also detected at the ciliary base (Fig. S3B,E), but recruitment of Ap80 to the centrosome or the ciliary base was independent of KIF13B (Fig. S3C,D). The localization of GFP-tagged (Fig. 3B) and endogenous PALS1 (Fig. S3F) was mostly dispersed in RPE1 cells, but upon co-expression with FLAG–Ap80 (Fig. 3C) or GFP–Ap80 (Fig. S3G), PALS1 accumulated at the ciliary base and at cytoplasmic Ap80-positive puncta. Consistent with our biochemical data, GFP–Ap80 and endogenous PALS1 colocalized with KIF13B-Δmotor–HA in intracellular puncta (Fig. S3H). Taken together, these results indicate that Ap80, KIF13B and PALS1 colocalize within cells, that Ap80 recruits PALS1 to the ciliary base and that Ap80 is likely not a cargo of KIF13B. Interestingly, in Madin–Darby canine kidney (MDCK)-II cells stably expressing PALS1 fused to APEX2–EGFP (hereby referred to as PALS1–A2E) (Tan et al., 2020), a fraction of PALS1–A2E was localized in a ring-like pattern around the ciliary base (Fig. S3I), and upon proximity biotinylation with APEX2 (labeling time <1 min), biotinylated proteins were found at the proximal regions of the primary cilium (Fig. S3J). This suggests that PALS1 dynamically shuttles between the periciliary membrane and proximal regions of the primary cilium and that the mechanism described here in RPE1 cells might be conserved in other cell types such as MDCK-II.

Ap80 regulates ciliary length and signaling in RPE1 cells

Next, we knocked out the *AMOT* gene (coding for Ap80 and Ap130) in RPE1 cells using the CRISPR/Cas9 system (Ran et al., 2013). We generated a clonal *AMOT*$^{-/-}$ line containing a homozygous 1 bp deletion in the first exon, resulting in a premature stop codon between positions 184 and 186 (Fig. S4A), which abolished the expression of the Ap80 protein (Fig. 3D). Interestingly, IFM with antibodies against ciliary markers revealed that *AMOT*$^{-/-}$ RPE1 cells have significantly longer cilia than wild-type (WT) cells (Fig. 3E,F). The *AMOT*$^{-/-}$ cells also seemed to undergo ciliogenesis less frequently than control cells, but this difference was statistically insignificant (Fig. S4B). Depletion of Ap80 using endoribonuclease-prepared small interfering RNA (esiRNA) recapitulated the long cilia phenotype of *AMOT*$^{-/-}$ cells (Fig. S4C–E). Conversely, cells expressing GFP–Ap80 had significantly shorter cilia, but similar ciliation frequency, compared to GFP-expressing cells (Fig. 3G,H; Fig. S4F). This was not due to protein over-expression as the average expression levels of GFP–Ap80 were about five times lower (18.2±2.0%, n=3) than those of GFP (100%, n=3), whereas transfection efficiencies were 25.1±7.2% (n=3) for GFP–Ap80 and 58.8±6.0% (n=3) for GFP, respectively. Finally, analysis of ciliary SMO accumulation in response to treatment with the SMO agonist purmorphamine (Sinha and Chen, 2006) showed significantly reduced ciliary levels of SMO in *AMOT*$^{-/-}$ cells compared to those seen in WT cells (Fig. 3I,J), indicative of defective Hedgehog signaling (Corbit et al., 2005). The *AMOT*$^{-/-}$ cells also had decreased cellular levels of AKT kinases (Fig. S4G). Other angiomotin family members also regulate AKT protein levels (Han et al., 2017; Ma et al., 2019), however, the underlying mechanisms and the specific role of AKT in the regulation of ciliary signaling remain to be investigated.

Conclusion

We characterized Ap80 as a KIF13B interactor that promotes binding of KIF13B to PALS1, and found that Ap80 is localized to the ciliary base where it recruits PALS1, controls ciliary length and promotes purmorphamine-induced SMO accumulation. Previously, Ap80 was shown to bind to RICH1, a GTPase-activating protein for the Rho GTPases CDC42 and RAC1 (Richnau and Aspenstrom, 2001), and mediate its targeting to epithelial tight junctions (Wells et al., 2006). This promoted the re-localization of PALS1, PATJ and PAR3 from tight junctions to apical early or recycling endosomes, perturbing tight junction integrity (Wells et al., 2006; Heller et al., 2010). A similar function for Ap80 was proposed in endothelial cells (Bratt et al., 2005; Levchenko et al., 2004; Troyanovsky et al., 2001). Our results suggest that Ap80 additionally controls the trafficking of PALS1 to the ciliary base, in turn affecting ciliary composition and function.

In both RPE1 and MDCK-II cells, PALS1 localized in a ring-like pattern around the ciliary base. This is reminiscent of a previously reported pericellular ring in MDCK cells that serves as a hotspot for the delivery of certain apical membrane proteins, such as gp135 (also known as podocalyxin or PODXL) (Stoops et al., 2015). Interestingly, following periciliary delivery, gp135 undergoes microtubule-dependent radial movement away from this region towards cell junctions (Stoops et al., 2015). Similarly, Ap80 and KIF13B might control periciliary PALS1 homeostasis by regulating both its recruitment to and movement away from the ciliary base. An alternative and non-exclusive possibility is that Ap80 and KIF13B promote PALS1 entry into the cilium itself. Indeed, KIF13B moves bidirectionally within the cilia of RPE1 cells (Juhl et al., 2023), and proximity biotinylation in PALS1–A2E MDCK-II cells indicated that PALS1 dynamically localizes to the proximal regions of the primary cilium, in addition to the periciliary membrane compartment.

We also found that *AMOT*$^{-/-}$ cells display decreased agonist-induced ciliary accumulation of SMO. Interestingly, in conditional *Pals1* knockout mice expressing a constitutively active *SmoM2* allele, the normally highly activated cerebellar Shh signaling response seen upon SmoM2 expression was abrogated, implicating Pals1 in the regulation of Shh signaling (Park et al., 2016). Upon activation of Shh signaling, Smo is transported laterally from the plasma membrane to the cilium (Milenkovic et al.,

Journal of Cell Science (2022) 135, jcs259471. doi:10.1242/jcs.259471

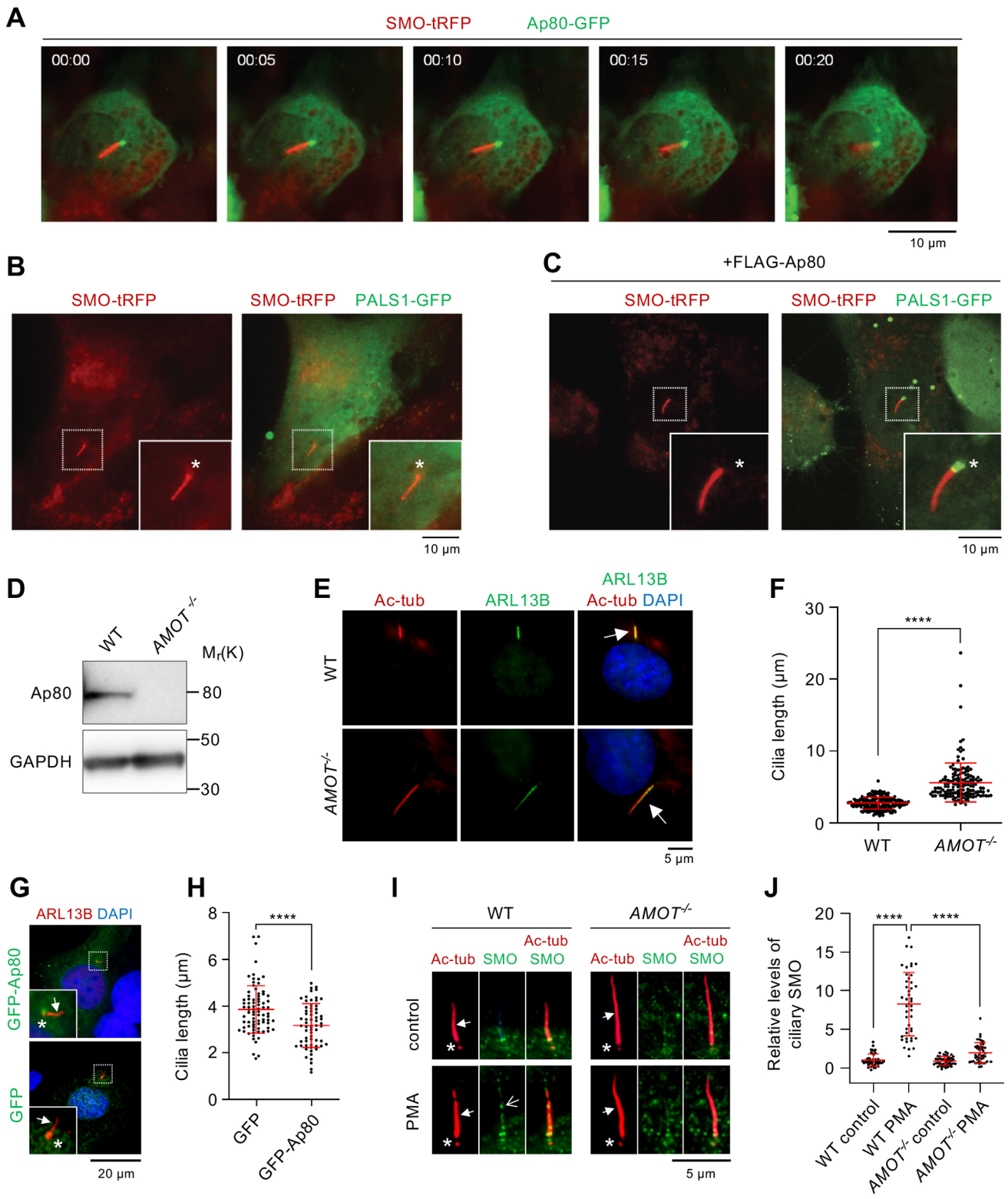

Fig. 3. Ap80 localizes to the ciliary base and regulates ciliary length in RPE1 cells. (A) Images from a time-lapse movie of a cell co-expressing SMO–tRFP and Ap80–GFP. Time is shown in seconds. (B,C) Images of live cells co-expressing SMO–tRFP and PALS1–GFP in the absence (B) or presence (C) of FLAG–Ap80. (D) Immunoblot of WT and *AMOT*$^{-/-}$ cells using the indicated antibodies. GAPDH was used as a loading control. (E) IFM images of serum-deprived WT (parental) and *AMOT*$^{-/-}$ cells using acetylated α-tubulin (AcTub) and ARL13B as ciliary markers (arrows). DNA was stained with DAPI. (F) Cilium length quantification in WT and *AMOT*$^{-/-}$ cells; >69 cilia measured in total per condition (n=3). (G,H) IFM images (G) and cilium length quantification (H) in GFP- or GFP–Ap80-expressing cells; 18–35 cilia were measured per condition per experiment (n=3). (I,J) IFM images (I) and quantification of relative ciliary SMO levels (J) in WT and *AMOT*$^{-/-}$ cells without (control) or with purmorphamine (PMA) stimulation. Fifteen cilia were measured per condition per experiment (n=3). Data in F, H and J show the mean±s.d. ****P≤0.0001 (unpaired two-tailed Student's t-test). Asterisks in images indicate the ciliary base, closed arrows indicate the cilia and the open arrow (I) indicates ciliary SMO accumulation. Scale bars: 10 µm (A–C), 5 µm (E,I), 20 µm (G).

2009). Therefore, we speculate that Ap80 and PALS1 jointly promote lateral transport of SMO to the ciliary base under these conditions.

Finally, although it remains to be clarified how Ap80 regulates ciliary length, this could be via its effects on actin dynamics (Kim et al., 2010), as Ap80 (Wells et al., 2006), KIF13B (Venkateswarlu et al., 2005; Kanai et al., 2014) and PALS1 (Lüttgenau et al., 2021) all interact with actin regulators. It will be interesting to investigate this further in future studies.

MATERIALS AND METHODS

Antibodies

For immunoblotting, the following primary antibodies were used (catalog numbers and dilutions in parenthesis): rabbit anti-FLAG (Sigma-Aldrich, F7425; 1:1000), rabbit anti-GFP (Santa Cruz Biotechnology, sc-8334; 1:1000), rabbit anti-HA (Santa Cruz Biotechnology, sc-805; 1:500), mouse anti-KIF13B (Sigma-Aldrich, SAB1412812; 1:500), mouse anti-α-tubulin (Sigma-Aldrich, T5168; 1:5000), rabbit anti-GAPDH (Cell Signaling Technology, 2118S; 1:1000), rabbit anti-AMOT (kindly provided by Dr Joseph Kissil, Scripps Research Institute, Jupiter, FL, USA; 1:1000) and rabbit anti-AKT (Cell Signaling Technology, 9272; 1:1000). The following secondary antibodies were used for immunoblotting: horseradish peroxidase (HRP)-conjugated swine anti-rabbit (Agilent Dako, P0399; 1:4000) and goat anti-mouse (Agilent Dako, P0447; 1:4000).

For IFM analysis, the following primary antibodies were used: mouse anti-FLAG (Sigma-Aldrich, F1804; 1:1000), mouse anti-PALS1 (Santa Cruz Biotechnology, sc-365411; 1:50), chicken anti-GFP (Abcam, ab13970; 1:2000), rabbit anti-ARL13B (Proteintech, 17711-1-AP; 1:500), mouse anti-acetylated α-tubulin (Sigma-Aldrich, T7451; 1:2000), rabbit anti-CEP164 (Sigma-Aldrich, HPA037606; 1:500), rabbit anti-HA (Santa Cruz Biotechnology, sc-805, 1:250), rabbit anti-SMO (Proteintech, 20787-1-AP; 1:500). The following secondary antibodies were used for IFM (all from Invitrogen and diluted 1:600): Alexa Fluor 488-conjugated donkey anti-mouse (A-21202), donkey anti-goat (A-11055), donkey anti-rabbit (A-21206) and goat anti-chicken (A11039); Alexa Fluor 568-conjugated donkey anti-mouse (A-10037) and donkey anti-rabbit (A-10042); Alexa Fluor 647-conjugated donkey anti-mouse (A-31571) and donkey anti-rabbit (A-31573).

PCR, cloning procedures and plasmids

All PCRs and cloning were performed following standard procedures; primer sequences are listed in Table S1 and plasmids used are listed in Table S2. Plasmids encoding the truncated versions of GFP–KIF13B (Tails 7, 8, 9, 11 and 12) were generated by PCR using the relevant primers and pEGFP-C1-KIF13B as a template (Asaba et al., 2003), followed by cloning into pEGFP-C1 (Clontech). Plasmids encoding truncated KIF13B–HA fusions (Tails 1 and 16) were generated by PCR using the relevant primers and pcDNA3-KIF13B-HA plasmid (Lamason et al., 2010) as a template. Plasmids encoding truncated versions of FLAG–Ap80 (-NB, -B, -C and -BC) were generated by PCR using the relevant primers and pCMV-Ap80 as a template, followed by cloning into pFLAG-CMV2 (Sigma-Aldrich). Plasmids encoding GFP–Ap80 or Ap80–GFP were generated by PCR using the relevant primers and pCMV-Ap80 as a template, followed by cloning into pEGFP-C1 or pEGFP-N1, respectively (Clontech). For CRISPR/Cas9-mediated knockout of *AMOT*, 25 nt oligos targeting exon 1 in *AMOT* (5′-AATACCGTGGTCCCTCCACTTGG-3′) were cloned into pSpCas9(BB)-2A-Puro (PX459) using the procedure described in Ran et al. (2013). *Escherichia coli* DH10B was used for transformation and plasmid amplification. Plasmid purification was performed using the NucleoBond Xtra Midi EF Kit from Macherey-Nagel. Inserts were sequenced at Eurofins MWG Operon, Ebersberg, Germany.

Cell culture and transfections

Unless otherwise stated, cells were grown at 37°C, with 5% CO_2 and 95% humidity in Dulbecco's modified Eagle's medium (DMEM, Gibco) with 10% heat-inactivated fetal bovine serum (FBS, Gibco) and 10 ml l^{-1} penicillin-streptomycin (Gibco), and cell cultures were passaged every 3–4 days. The following cell lines were used: HEK293T cells [laboratory stock, originally derived from American Type culture collection (ATCC), clone CRL-3216]; hTERT-RPE1 cells (laboratory stock; originally derived from the immortalized hTERT-RPE1 cell line, ATCC, clone CRL-4000); hTERT-RPE1 cells lacking KIF13B (*KIF13B*$^{-/-}$; Schou et al., 2017); hTERT-RPE1 cells stably expressing SMO-tRFP (Lu et al., 2015); Swiss NIH3T3 mouse fibroblasts (laboratory stock, originally derived from the ATCC clone CRL-1658); mouse inner medullary collecting duct (IMCD3) cells (laboratory stock, originally derived from the ATCC clone CRL-2123); and PALS1–A2E MDCK-II cells (Tan et al., 2020). IMCD3 cells were grown in 45% DMEM and 45% F-12 (Ham; Sigma-Aldrich) with 10% FBS and 10 ml l^{-1} penicillin-streptomycin, whereas the PALS1-A2E MDCK-II cells were grown and subjected to APEX2-mediated biotinylation as described previously (Tan et al., 2020). The *AMOT*$^{-/-}$ RPE1 clone was generated using the CRISPR/Cas9 method described in Ran et al. (2013) using the plasmid pSpCas9(BB)-2A-Puro (PX459) encoding *AMOT*-specific guide RNA targeting the first exon of *AMOT* (5′-AATACCGTGGTCCCTC-CACTTGG-3′). Screening of 91 clones by immunoblot analysis led to the identification of a single clone with no detectable Ap80 expression. Sequencing of PCR-amplified genomic DNA from this clone revealed a 1 bp deletion in exon 1 resulting in a premature stop codon.

For induction of Shh signaling, serum-deprived WT and *AMOT*$^{-/-}$ RPE1 cells were incubated with 1 µM purmorphamine (Sigma-Aldrich, SML0868) or an equivalent volume of vehicle (DMSO; control) for 24 h prior to IFM.

For plasmid transfections, cells were grown to 40–50% confluency and transfections were performed using FuGene6 (Promega, E2692) according to the manufacturer's protocol. For IP experiments, HEK293T cells were grown in 10 cm-diameter Petri dishes and transfected with 4 µg DNA. Six hours after transfection, the medium was changed to fresh growth medium and the cells were incubated for 16 h before harvesting. For IFM experiments, RPE1 cells were grown on glass coverslips in 20 mm-diameter dishes and transfected with 1 µg DNA. Six hours after transfection, the medium was changed to either growth or serum-deprived medium for 16–24 h. For immunoblot experiments, RPE1 cells were grown in 60 mm-diameter dishes and transfected with 2 µg DNA. Six hours after transfection, the medium was changed to either growth or serum-deprived medium for 16–24 h.

All transfections with esiRNA (Sigma-Aldrich, MISSION esiRNA targeting human *AMOT*; EHU129771) and control siRNA [5′-UAAU-GUAUUGGAAUGCAUA(dTdT)-3′, Eurofins MWG Operon] were performed as double transfections using DharmaFECT Duo (Dharmacon). RPE1 cells were grown to 80% confluency and transfected according to the manufacturer's protocol. Six hours after transfection, the medium was changed to fresh growth medium. The following day, the cells were transfected again. After 36 h, the cells were split and an appropriate number of cells were seeded for IFM or immunoblot analysis. Prior to fixation or cell lysis, the cells were serum-deprived for 16–24 h.

Streptavidin pull-down assays and mass spectrometry

HEK293T cells were transfected with BirAGFP–KIF13B Tail 2 or Tail 3 constructs [designated C2 and C3, respectively, in Serra-Marques et al. (2020)] using polyethylenimine (PEI; MW 2500; Polysciences) at a 3:1 PEI: DNA ratio (w/w). Cells were harvested 24 h after transfection by scraping in ice-cold PBS, centrifugation for 5 min at 2000 ***g*** and lysing cell pellets in the lysis buffer [20 mM Tris-HCl (pH 7.5), 100 mM NaCl, 1.0% Triton X-100 and protease inhibitors (Roche)]. Supernatants and pellet fractions were separated by centrifugation at 16,000 ***g*** for 20 min. Supernatants were then mixed with an equal amount of Dyna M-280 Streptavidin beads (Life Technologies). Samples were incubated for 2 h while rotating at 4°C, the beads collected with a magnet and pellets washed five to seven times with the wash buffer [20 mM Tris-HCl (pH 7.5), 100 mM NaCl, 0.1% Triton X-100]. Samples were eluted in SDS sample buffer and 30 µl of each sample was run on a 12% bis-tris 1D SDS-PAGE gel (Bio-Rad) for 1 cm and stained with colloidal Coomassie G-250 (GelCode Blue Stain Reagent, Thermo Fisher Scientific). Each lane was cut into one band, which was treated with 6.5 mM dithiothreitol for 1 h at 60°C for reduction and 54 mM iodoacetamide for 30 min for alkylation. The proteins were digested overnight with trypsin (Promega) at 37°C. The peptides were extracted with

acetonitrile and dried in a vacuum concentrator. The data were acquired using an Orbitrap Q Exactive mass spectrometer. Peptides were first trapped (Dr Maisch, ReproSil-Pur Basic-C18, 3 µm, 2 cm×100 µm) before being separated on an analytical column (Zorbax SB-C18, 1.8 µm, 40 cm×50 µm) using a gradient elution for 60 min at a column flow of 150 nl min^{-1}. Trapping was performed at 8 µl/min for 10 min in solvent A (0.1 M acetic acid in water) and the gradient elution protocol was as follows: a gradient increasing from 7% to 30% solvent B (0.1 M acetic acid in acetonitrile) in 31 min, a gradient increasing from 30% to 100% in the next 3 min, 100% solvent B for 5 min and 7% solvent B for 13 min. Full scan MS spectra for a mass-to-charge ratio (m/z) between 350 and 1500 were acquired at a resolution of 35,000 at m/z 400, after ion accumulation to a target value of 3×10^6. Up to ten most intense precursor ions were selected for fragmentation. Higher-energy C-trap dissociation (HCD) fragmentation was performed at a normalized collision energy of 25% after the accumulation to a target value of 5×10^4. Tandem mass spectrometry (MS/MS) spectra were acquired at a resolution of 17,500. In all cases, nano-electrospray ionization was performed at 1.7 kV using an in-house-made, gold-coated, fused silica capillary (outer diameter, 360 µm; inner diameter, 20 µm; tip inner diameter, 10 µm). Raw files were processed using Proteome Discoverer 1.3 (Thermo Fisher Scientific, Bremen, Germany). The database search was performed against the Swiss-Prot human database, taxonomy (version November 2012) using Mascot (version 2.3, Matrix Science, UK) as search engine. Carbamidomethylation of cysteines was set as a fixed modification and oxidation of methionine was set as a variable modification. Trypsin was specified as the enzyme and up to two missed cleavages were allowed. Data filtering was performed using Percolator, resulting in a 1% false discovery rate (FDR). An additional filter was Mascot ion score >20. Raw files corresponding to one sample were merged into one result file.

Immunoprecipitation

HEK293T cells were transfected with the relevant plasmids 24 h before IP. Cells were then harvested using ice-cold EBC buffer [140 mM NaCl, 50 mM Tris-HCl, 0.5% NP-40, 5 mM EDTA and protease inhibitor cocktail (Roche)] and briefly sonicated, followed by centrifugation for 20 min at 20,000 ***g*** at 4°C. For FLAG, GFP and HA IP, cleared cell lysates were incubated for 1 h at 4°C while rotating with 20 µl bead slurry of anti-FLAG (M2)-conjugated beads (Sigma-Aldrich, A2220), 25 µl bead slurry of GFP-Trap A beads (ChromoTek, gta-20) or 20 µl bead slurry of Pierce™ Anti-HA Agarose Conjugate (Thermo Fisher Scientific, 26181), respectively. The immunocomplexes were washed four times with EBC buffer and eluted with SDS-PAGE sample buffer. The eluted proteins were then subjected to SDS-PAGE and immunoblotting. All IP experiments were repeated independently at least three times, and figures show representative results from these independent repeats.

Protein concentration determination, SDS-PAGE and immunoblotting

The Bio-Rad DC Protein Assay was used to determine the protein concentration of cell lysates. SDS-PAGE and immunoblotting were performed as previously described (Schou et al., 2017). Original immunoblots are shown in Fig. S5.

Immunofluorescence microscopy

For IFM analysis, RPE1 cells were grown on glass coverslips, and subjected to 16–24 h serum-deprivation to induce ciliogenesis. Cells were washed in ice-cold PBS, fixed with 4% paraformaldehyde solution for 15 min at room temperature (RT) and cell membranes were permeabilized by incubation with 1% (w/v) bovine serum albumin (BSA) and 0.2% (v/v) Triton X-100 in 1× PBS for 12 min at RT. A blocking step of 30 min incubation at RT with 2% BSA in 1× PBS was performed to avoid non-specific binding of antibodies, followed by incubation with primary antibodies overnight at 4°C. After three washing steps with 2% BSA in 1× PBS, cells were incubated with the appropriate Alexa Fluor-conjugated secondary antibodies that were diluted in 2% BSA in 1× PBS for 45 min at RT, and nuclei were labeled with DAPI. Coverslips were mounted using 90% glycerol and 2% n-propyl gallate in 1× PBS on glass slides and the edges were sealed with nail polish. Fluorescence images were captured on a fully motorized Olympus BX63 upright microscope with an Olympus DP72 color, 12.8-megapixel, 4140×3096 resolution camera and with a fully motorized and automated Olympus IX83 inverted microscope with a Hamamatsu ORCA-Flash 4.0 camera (C11440-22CU). The software used was Olympus CellSens dimension. Images were processed for publication using Adobe Photoshop version CS6. For quantifications of the centrosomal FLAG–Ap80 and ciliary SMO levels, images were analyzed using ImageJ and Olympus CellSens, respectively. Outlines were drawn around each centrosome or cilium and, using the measurement and integrated density functions, the mean fluorescence intensity (MFI) was measured in these areas along with background readings. The corrected MFI in the centrosome and the cilium was calculated by subtracting the corresponding background value. Procedures for confocal microscopy analysis of PALS1–A2E MDCK-II cells are described in Tan et al. (2020).

Live-cell fluorescence imaging

Transfection and live-cell imaging of RPE1 cells stably expressing SMO–tRFP were performed as described previously (Juhl et al., 2023). Live-cell imaging of Ap80–GFP and mCherry–KIF13B was performed using total internal reflection fluorescence (TIRF) microscopy with the inverted research microscope Nikon Eclipse Ti-E (Nikon), equipped with the perfect focus system (Nikon), Nikon Apo TIRF 100× N.A. 1.49 oil objective (Nikon) and iLas3 system [Dual Laser illuminator for azimuthal spinning TIRF (or Oblique) illumination and Simultaneous Targeted Laser Action including PhotoAblation; Gataca Systems]. The system was also equipped with the ASI motorized stage MS-2000-XY (ASI), Photometrics Evolve 512 Delta EMCCD back-illuminated camera (Teledyne Photometrics) and controlled by the MetaMorph 7.8 software (Molecular Devices). Stradus 488 nm (150 mW, Vortran) and OBIS 561 nm (100 mW, Coherent) lasers were used as the light sources. We used the ZT405/488/561/640rpc ZET405/488/561/635 m filter set (TRF89901, Chroma) together with the Optosplit III beamsplitter (Cairn Research Ltd, UK) equipped with a double emission filter cube configured with ET525/50 m, ET630/75 m and T585LPXR (Chroma). 16-bit images were projected onto the EMCCD chip with intermediate lens 2.5× (Nikon C mount adapter 2.5×) at a magnification of 0.065 µm/pixel. To maintain the cells at 37°C, we used a stage top incubator (model INUBG2E-ZILCS, Tokai Hit).

Statistical analysis

Statistical analysis was performed using GraphPad Prism 6 software.

Acknowledgements

We thank Søren Johansen, Maria Holm, Emilie Baldram, Ida Hemmingsen, Signe Aagard and Sara Enevoldsen for technical assistance, and Joseph Kissil, Athar Chisthi, Joel Pomerantz, Sadanori Watanabe, Hiroaki Miki, Ronald Roepman, Francesc Garcia-Gonzalo, Lars Ellgaard, Dannel McCollum, Christopher Westlake and Jeffrey Miner for reagents.

Competing interests

The authors declare no competing or financial interests.

Author contributions

Conceptualization: P.F., L.B.P.; Methodology: S.K.M., C.N., P.F., Z.A., A.S.-M., I.G., M.A., N.F., A.L.; Validation: C.N., P.F., C.B.R.R.; Formal analysis: S.K.M., C.N., P.F., Z.A., C.B.R.R., A.S.-M., I.G., N.F., A.L., A.A., S.T.C.; Investigation: S.K.M., C.N., P.F., Z.A., C.B.R.R., A.S.-M., I.G., M.A., N.F., A.L.; Data curation: M.A.; Writing - original draft: S.K.M., S.T.C., L.B.P.; Writing - review & editing: S.K.M., A.S.-M., A.L., A.A., S.T.C., L.B.P.; Visualization: S.K.M., C.N., P.F., Z.A., C.B.R.R., I.G., A.L., A.A., S.T.C., L.B.P.; Supervision: A.A., L.B.P.; Project administration: L.B.P.; Funding acquisition: A.A., L.B.P.

Funding

This work was supported by grants from Novo Nordisk Fonden (NNF14OC0011535, NNF15OC0016886), Hartmann Fonden (A31662), Kræftens Bekæmpelse (R146-A9590), Københavns Universitet (University of Copenhagen, UCPH) Excellence Programme for Interdisciplinary Research to L.B.P. and S.T.C., the Danmarks Frie Forskningsfond (6108-00457B) to S.T.C. and the Ministry of Education - Singapore (MOE 2019-T1-002-097) to A.L. S.K.M. was partially supported by a PhD fellowship from the Department of Biology, Københavns Universitet. A.A. was supported by the Netherlands X-omics Initiative partially funded by Nederlandse Organisatie voor Wetenschappelijk Onderzoek (project 184.034.019).

Peer review history
The peer review history is available online at https://journals.biologists.com/jcs/article-lookup/doi/10.1242/jcs.259471.

References

Akella, J. S. and Barr, M. M. (2021). The tubulin code specializes neuronal cilia for extracellular vesicle release. *Dev. Neurobiol.* **81**, 231-252. doi:10.1002/dneu.22787

Anvarian, Z., Mykytyn, K., Mukhopadhyay, S., Pedersen, L. B. and Christensen, S. T. (2019). Cellular signalling by primary cilia in development, organ function and disease. *Nat. Rev. Nephrol.* **15**, 199-219. doi:10.1038/s41581-019-0116-9

Asaba, N., Hanada, T., Takeuchi, A. and Chishti, A. H. (2003). Direct interaction with a Kinesin-related motor mediates transport of mammalian discs large tumor suppressor homologue in epithelial cells. *J. Biol. Chem.* **278**, 8395-8400. doi:10.1074/jbc.M210362200

Bangs, F. and Anderson, K. V. (2017). Primary cilia and mammalian hedgehog signaling. *Cold Spring Harb. Perspect. Biol.* **9**, a028175. doi:10.1101/cshperspect.a028175

Bohl, J., Brimer, N., Lyons, C. and Vande Pol, S. B. (2007). The stardust family protein MPP7 forms a tripartite complex with LIN7 and DLG1 that regulates the stability and localization of DLG1 to cell junctions. *J. Biol. Chem.* **282**, 9392-9400. doi:10.1074/jbc.M610002200

Bolis, A., Coviello, S., Visigalli, I., Taveggia, C., Bachi, A., Chishti, A. H., Hanada, T., Quattrini, A., Previtali, S. C., Biffi, A. et al. (2009). Dlg1, Sec8, and Mtmr2 regulate membrane homeostasis in Schwann cell myelination. *J. Neurosci.* **29**, 8858-8870. doi:10.1523/JNEUROSCI.1423-09.2009

Bratt, A., Birot, O., Sinha, I., Veitonmäki, N., Aase, K., Ernkvist, M. and Holmgren, L. (2005). Angiomotin regulates endothelial cell-cell junctions and cell motility. *J. Biol. Chem.* **280**, 34859-34869. doi:10.1074/jbc.M503915200

Corbit, K. C., Aanstad, P., Singla, V., Norman, A. R., Stainier, D. Y. R. and Reiter, J. F. (2005). Vertebrate smoothened functions at the primary cilium. *Nature* **437**, 1018-1021. doi:10.1038/nature04117

Delous, M., Hellman, N. E., Gaudé, H.-M., Silbermann, F., Le Bivic, A., Salomon, R., Antignac, C. and Saunier, S. (2009). Nephrocystin-1 and nephrocystin-4 are required for epithelial morphogenesis and associate with PALS1/PATJ and Par6. *Hum. Mol. Genet.* **18**, 4711-4723. doi:10.1093/hmg/ddp434

Ernkvist, M., Aase, K., Ukomadu, C., Wohlschlegel, J., Blackman, R., Veitonmäki, N., Bratt, A., Dutta, A. and Holmgren, L. (2006). p130-angiomotin associates to actin and controls endothelial cell shape. *FEBS J.* **273**, 2000-2011. doi:10.1111/j.1742-4658.2006.05216.x

Garcia-Gonzalo, F. R. and Reiter, J. F. (2017). Open sesame: how transition fibers and the transition zone control ciliary composition. *Cold Spring Harb. Perspect. Biol.* **9**, a028134. doi:10.1101/cshperspect.a028134

Han, H., Yang, B. and Wang, W. (2017). Angiomotin-like 2 interacts with and negatively regulates AKT. *Oncogene* **36**, 4662-4669. doi:10.1038/onc.2017.101

Hanada, T., Lin, L., Tibaldi, E. V., Reinherz, E. L. and Chishti, A. H. (2000). GAKIN, a novel kinesin-like protein associates with the human homologue of the Drosophila discs large tumor suppressor in T lymphocytes. *J. Biol. Chem.* **275**, 28774-28784. doi:10.1074/jbc.M000715200

Heller, B., Adu-Gyamfi, E., Smith-Kinnaman, W., Babbey, C., Vora, M., Xue, Y., Bittman, R., Stahelin, R. V. and Wells, C. D. (2010). Amot recognizes a juxtanuclear endocytic recycling compartment via a novel lipid binding domain. *J. Biol. Chem.* **285**, 12308-12320. doi:10.1074/jbc.M109.096230

Horiguchi, K., Hanada, T., Fukui, Y. and Chishti, A. H. (2006). Transport of PIP_3 by GAKIN, a kinesin-3 family protein, regulates neuronal cell polarity. *J. Cell Biol.* **174**, 425-436. doi:10.1083/jcb.200604031

Juhl, A. D., Anvarian, Z., Kuhns, S., Berges, J., Andersen, J. S., Wüstner, D. and Pedersen, L. B. (2023). Transient accumulation and bidirectional movement of KIF13B in primary cilia. *J. Cell Sci.* **136**, jcs259257. doi:10.1242/jcs.259257

Kanai, Y., Wang, D. and Hirokawa, N. (2014). KIF13B enhances the endocytosis of LRP1 by recruiting LRP1 to caveolae. *J. Cell Biol.* **204**, 395-408. doi:10.1083/jcb.201309066

Kim, J., Lee, J. E., Heynen-Genel, S., Suyama, E., Ono, K., Lee, K., Ideker, T., Aza-Blanc, P. and Gleeson, J. G. (2010). Functional genomic screen for modulators of ciliogenesis and cilium length. *Nature* **464**, 1048-1051. doi:10.1038/nature08895

Kramarcy, N. R., Vidal, A., Froehner, S. C. and Sealock, R. (1994). Association of utrophin and multiple dystrophin short forms with the mammalian M(r) 58,000 dystrophin-associated protein (syntrophin). *J. Biol. Chem.* **269**, 2870-2876. doi:10.1016/S0021-9258(17)42023-0

Lamason, R. L., Kupfer, A. and Pomerantz, J. L. (2010). The dynamic distribution of CARD11 at the immunological synapse is regulated by the inhibitory kinesin GAKIN. *Mol. Cell* **40**, 798-809. doi:10.1016/j.molcel.2010.11.007

Lee, S., Fan, S., Makarova, O., Straight, S. and Margolis, B. (2002). A novel and conserved protein-protein interaction domain of mammalian Lin-2/CASK binds and recruits SAP97 to the lateral surface of epithelia. *Mol. Cell. Biol.* **22**, 1778-1791. doi:10.1128/MCB.22.6.1778-1791.2002

Levchenko, T., Bratt, A., Arbiser, J. L. and Holmgren, L. (2004). Angiomotin expression promotes hemangioendothelioma invasion. *Oncogene* **23**, 1469-1473. doi:10.1038/sj.onc.1207264

Lu, Q., Insinna, C., Ott, C., Stauffer, J., Pintado, P. A., Rahajeng, J., Baxa, U., Walia, V., Cuenca, A., Hwang, Y. S. et al. (2015). Early steps in primary cilium assembly require EHD1/EHD3-dependent ciliary vesicle formation. *Nat. Cell Biol.* **17**, 228-240. doi:10.1038/ncb3109

Lüttgenau, S. M., Emming, C., Wagner, T., Harms, J., Guske, J., Weber, K., Neugebauer, U., Schröter, R., Panichkina, O., Pethő, Z. et al. (2021). Pals1 prevents Rac1-dependent colorectal cancer cell metastasis by inhibiting Arf6. *Mol. Cancer* **20**, 74. doi:10.1186/s12943-021-01354-2

Ma, J., Fang, L., Yang, Q., Hibberd, S., Du, W. W., Wu, N. and Yang, B. B. (2019). Posttranscriptional regulation of AKT by circular RNA angiomotin- like 1 mediates chemoresistance against paclitaxel in breast cancer cells. *Aging* **11**, 11369-11381. doi:10.18632/aging.102535

Milenkovic, L., Scott, M. P. and Rohatgi, R. (2009). Lateral transport of Smoothened from the plasma membrane to the membrane of the cilium. *J. Cell Biol.* **187**, 365-374. doi:10.1083/jcb.200907126

Mills, J., Hanada, T., Hase, Y., Liscum, L. and Chishti, A. H. (2019). LDL receptor related protein 1 requires the I3 domain of discs-large homolog 1/DLG1 for interaction with the Kinesin motor protein KIF13B. *Biochim. Biophys. Acta. Mol. Cell Res.* **1866**, 118552. doi:10.1016/j.bbamcr.2019.118552

Moleirinho, S., Guerrant, W. and Kissil, J. L. (2014). The angiomotins - from discovery to function. *FEBS Lett.* **588**, 2693-2703. doi:10.1016/j.febslet.2014.02.006

Morthorst, S. K., Christensen, S. T. and Pedersen, L. B. (2018). Regulation of ciliary membrane protein trafficking and signalling by kinesin motor proteins. *FEBS J.* **285**, 4535-4564. doi:10.1111/febs.14583

Neubrand, V. E., Cesca, F., Benfenati, F. and Schiavo, G. (2012). Kidins220/ARMS as a functional mediator of multiple receptor signalling pathways. *J. Cell Sci.* **125**, 1845-1854. doi:10.1242/jcs.102764

Noseda, R., Guerrero-Valero, M., Alberizzi, V., Previtali, S. C., Sherman, D. L., Palmisano, M., Huganir, R. L., Nave, K. A., Cuenda, A., Feltri, M. L. et al. (2016). Kif13b regulates PNS and CNS myelination through the Dlg1 Scaffold. *PLoS Biol.* **14**, e1002440. doi:10.1371/journal.pbio.1002440

Ossipova, O., Chu, C.-W., Fillatre, J., Brott, B. K., Itoh, K. and Sokol, S. Y. (2015). The involvement of PCP proteins in radial cell intercalations during Xenopus embryonic development. *Dev. Biol.* **408**, 316-327. doi:10.1016/j.ydbio.2015.06.013

Park, J. Y., Hughes, L. J., Moon, U. Y., Park, R., Kim, S. B., Tran, K., Lee, J. S., Cho, S. H. and Kim, S. (2016). The apical complex protein Pals1 is required to maintain cerebellar progenitor cells in a proliferative state. *Development* **143**, 133-146. doi:10.1242/dev.124180

Peters, M. F., Adams, M. E. and Froehner, S. C. (1997). Differential association of syntrophin pairs with the dystrophin complex. *J. Cell Biol.* **138**, 81-93. doi:10.1083/jcb.138.1.81

Pugacheva, E. N., Jablonski, S. A., Hartman, T. R., Henske, E. P. and Golemis, E. A. (2007). HEF1-dependent Aurora A activation induces disassembly of the primary cilium. *Cell* **129**, 1351-1363. doi:10.1016/j.cell.2007.04.035

Ran, F. A., Hsu, P. D., Wright, J., Agarwala, V., Scott, D. A. and Zhang, F. (2013). Genome engineering using the CRISPR-Cas9 system. *Nat. Protoc.* **8**, 2281-2308. doi:10.1038/nprot.2013.143

Ren, J., Wang, S., Chen, H., Wang, W., Huo, L. and Feng, W. (2018). Coiled-coil 1-mediated fastening of the neck and motor domains for kinesin-3 autoinhibition. *Proc. Natl. Acad. Sci. USA* **115**, E11933-E11942. doi:10.1073/pnas.1811209115

Richnau, N. and Aspenström, P. (2001). Rich, a rho GTPase-activating protein domain-containing protein involved in signaling by Cdc42 and Rac1. *J. Biol. Chem.* **276**, 35060-35070. doi:10.1074/jbc.M103540200

Sang, L., Miller, J. J., Corbit, K. C., Giles, R. H., Brauer, M. J., Otto, E. A., Baye, L. M., Wen, X., Scales, S. J., Kwong, M. et al. (2011). Mapping the NPHP-JBTS-MKS protein network reveals ciliopathy disease genes and pathways. *Cell* **145**, 513-528. doi:10.1016/j.cell.2011.04.019

Schou, K. B., Mogensen, J. B., Morthorst, S. K., Nielsen, B. S., Aleliunaite, A., Serra-Marques, A., Fürstenberg, N., Saunier, S., Bizet, A. A., Veland, I. R. et al. (2017). KIF13B establishes a CAV1-enriched microdomain at the ciliary transition zone to promote Sonic hedgehog signalling. *Nat. Commun.* **8**, 14177. doi:10.1038/ncomms14177

Serra-Marques, A., Martin, M., Katrukha, E. A., Grigoriev, I., Peeters, C. A., Liu, Q., Hooikaas, P. J., Yao, Y., Solianova, V., Smal, I. et al. (2020). Concerted action of kinesins KIF5B and KIF13B promotes efficient secretory vesicle transport to microtubule plus ends. *Elife* **9**, e61302. doi:10.7554/eLife.61302

Siddiqui, N. and Straube, A. (2017). Intracellular cargo transport by kinesin-3 motors. *Biochemistry* **82**, 803-815. doi:10.1134/S0006297917070057

Sinha, S. and Chen, J. K. (2006). Purmorphamine activates the hedgehog pathway by targeting smoothened. *Nat. Chem. Biol.* **2**, 29-30. doi:10.1038/nchembio753

Soppina, V., Norris, S. R., Dizaji, A. S., Kortus, M., Veatch, S., Peckham, M. and Verhey, K. J. (2014). Dimerization of mammalian kinesin-3 motors results in superprocessive motion. *Proc. Natl. Acad. Sci. USA* **111**, 5562-5567. doi:10.1073/pnas.1400759111

Stoops, E. H., Hull, M., Olesen, C., Mistry, K., Harder, J. L., Rivera-Molina, F., Toomre, D. and Caplan, M. J. (2015). The periciliary ring in polarized epithelial cells is a hot spot for delivery of the apical protein gp135. *J. Cell Biol.* **211**, 287-294. doi:10.1083/jcb.201502045

Tan, B., Yatim, S., Peng, S., Gunaratne, J., Hunziker, W. and Ludwig, A. (2020). The mammalian crumbs complex defines a distinct polarity domain apical of epithelial tight junctions. *Curr. Biol.* **30**, 2791-2804.e6. doi:10.1016/j.cub.2020.05.032

Tarbashevich, K., Dzementsei, A. and Pieler, T. (2011). A novel function for KIF13B in germ cell migration. *Dev. Biol.* **349**, 169-178. doi:10.1016/j.ydbio.2010.10.016

Taschner, M. and Lorentzen, E. (2016). The intraflagellar transport machinery. *Cold Spring Harb. Perspect. Biol.* **8**, a028092. doi:10.1101/cshperspect.a028092

Troyanovsky, B., Levchenko, T., Månsson, G., Matvijenko, O. and Holmgren, L. (2001). Angiomotin: an angiostatin binding protein that regulates endothelial cell migration and tube formation. *J. Cell Biol.* **152**, 1247-1254. doi:10.1083/jcb.152.6.1247

Venkateswarlu, K., Hanada, T. and Chishti, A. H. (2005). Centaurin-α1 interacts directly with kinesin motor protein KIF13B. *J. Cell Sci.* **118**, 2471-2484. doi:10.1242/jcs.02369

Wells, C. D., Fawcett, J. P., Traweger, A., Yamanaka, Y., Goudreault, M., Elder, K., Kulkarni, S., Gish, G., Virag, C., Lim, C. et al. (2006). A Rich1/Amot complex regulates the Cdc42 GTPase and apical-polarity proteins in epithelial cells. *Cell* **125**, 535-548. doi:10.1016/j.cell.2006.02.045

Yamada, K. H., Hanada, T. and Chishti, A. H. (2007). The effector domain of human dlg tumor suppressor acts as a switch that relieves autoinhibition of kinesin-3 motor GAKIN/KIF13B. *Biochemistry* **46**, 10039-10045. doi:10.1021/bi701169w

Yamada, K. H., Nakajima, Y., Geyer, M., Wary, K. K., Ushio-Fukai, M., Komarova, Y. and Malik, A. B. (2014). KIF13B regulates angiogenesis through Golgi to plasma membrane trafficking of VEGFR2. *J. Cell Sci.* **127**, 4518-4530. doi:10.1242/jcs.156109

Yoshimura, Y., Terabayashi, T. and Miki, H. (2010). Par1b/MARK2 phosphorylates kinesin-like motor protein GAKIN/KIF13B to regulate axon formation. *Mol. Cell. Biol.* **30**, 2206-2219. doi:10.1128/MCB.01181-09

Zhu, J., Shang, Y., Xia, Y., Zhang, R. and Zhang, M. (2016). An atypical MAGUK GK target recognition mode revealed by the interaction between DLG and KIF13B. *Structure* **24**, 1876-1885. doi:10.1016/j.str.2016.08.008